



PAPER

Stationary multi-kinks in the discrete sine-Gordon equation

To cite this article: Ross Parker et al 2022 Nonlinearity 35 1036

View the <u>article online</u> for updates and enhancements.

You may also like

- <u>Multiply Kink and Anti-Kink Solutions for a Coupled Camassa—Holm Type Equation</u> Yuan-Li Li, , Qi-Lao Zha et al.
- <u>Forces between kinks in ⁸ theory</u> Peru d'Ornellas
- <u>Kink solutions in a generalized scalar ⁴</u> <u>field model</u>
 Jonathan Lozano-Mayo and Manuel
 Torres-Labansat

Stationary multi-kinks in the discrete sine-Gordon equation

Ross Parker^{1,*}, P G Kevrekidis² and Alejandro Aceves¹

- Department of Mathematics, Southern Methodist University, Dallas, TX 75275, United States of America
- ² Department of Mathematics and Statistics, University of Massachusetts, Amherst MA 01003, United States of America

E-mail: rhparker@smu.edu, kevrekid@math.umass.edu and aaceves@smu.edu

Received 16 July 2021, revised 24 November 2021 Accepted for publication 2 December 2021 Published 31 December 2021



Abstract

We consider the existence and spectral stability of static multi-kink structures in the discrete sine-Gordon equation, as a representative example of the family of discrete Klein–Gordon models. The multi-kinks are constructed using Lin's method from an alternating sequence of well-separated kink and antikink solutions. We then locate the point spectrum associated with these multi-kink solutions by reducing the spectral problem to a matrix equation. For an *m*-structure multi-kink, there will be *m* eigenvalues in the point spectrum near each eigenvalue of the primary kink, and, as long as the spectrum of the primary kink is imaginary, the spectrum of the multi-kink will be as well. We obtain analytic expressions for the eigenvalues of a multi-kink in terms of the eigenvalues and corresponding eigenfunctions of the primary kink, and these are in very good agreement with numerical results. We also perform numerical time-stepping experiments on perturbations of multi-kinks, and the outcomes of these simulations are interpreted using the spectral results.

Keywords: discrete sine-Gordon equation, discrete Hamiltonian systems, non-linear waves, dynamical systems

Mathematics Subject Classification numbers: 37K45, 37K60.

(Some figures may appear in colour only in the online journal)

^{*}Author to whom any correspondence should be addressed. Recommended by Dr Karima Khusnutdinova.

1. Introduction

The 1+1-dimensional nonlinear Klein–Gordon models have been one of the preeminent platforms where ideas from integrable, as well as near-integrable, theory of nonlinear partial differential equations and the corresponding solitary waves have been developed. This is by now evidenced by numerous monographs [1, 2], specialized books for these models [3–5] and reviews [6, 7]. Both continuum and discrete models of this kind have been of interest to physical applications, as well as to applied analysis, and their comparison as regards the transition from discrete to continuum has been of interest in its own right [8].

The discrete Klein-Gordon equation

$$\ddot{u}_n = d(\Delta_2 u)_n - f(u_n)$$

describes the dynamics of an infinitely long, one-dimensional lattice of particles which are harmonically coupled to their neighbors through the discrete second difference operator Δ_2 and are subject to an external, nonlinear, onsite potential P(u) such that f(u) = P'(u) [9]. The quantity u_n represents the displacement of the particle at site n in the lattice, d is the strength of the nearest neighbor coupling, and the dot denotes the derivative with respect to the time t.

A specific example is the discrete sine-Gordon equation

$$\ddot{u}_n = d(\Delta_2 u)_n \pm \sin(u_n),\tag{1}$$

in which the external potential is periodic. This equation is also known as the Frenkel–Kontorova model, and was introduced in 1938 to describe the dynamics of a crystal lattice near a dislocation core [3, 7]. This equation has since been used in numerous applications, including a mechanical model for a chain of pendula coupled with elastic springs [10, 11], arrays of Josephson junctions [12, 13], and DNA dynamics [14–16]. (See [3, chapter 2] for more physical applications of this model.) Another example of substantial interest is the discrete ϕ^4 model

$$\ddot{u}_n = d(\Delta_2 u)_n + 2u_n(1 - u_n^2),\tag{2}$$

which has a double well external potential, and has applications to conducting polymers [17]. In addition, the latter model has been a central point of focus as concerns the dynamics of discrete breathers, i.e. time-periodic and exponentially localized solutions in space [18, 19].

Equation (1) is the discrete analogue of the continuum sine-Gordon PDE

$$u_{tt} = u_{xx} \pm \sin(u), \tag{3}$$

which has many physical (including, e.g., fluxons in Josephson junctions, charge density waves in quasi-1D conducting materials, among many others) and biological applications [4, 20] and has been extensively studied both in the mathematical and physics literature due to the fact that it is integrable via the inverse scattering transform [21]. We note that if u(x) is a solution to (3) with the 'minus' nonlinearity, $u(x) - \pi$ is a solution with the 'plus' nonlinearity. The same holds for (1). For symmetry reasons, which will be explained in section 2, we will consider only the 'plus' nonlinearity here. Of particular interest are coherent structures such as kinks (figure 1, left panel), exponentially localized stationary solutions which are heteroclinic orbits that connect two adjacent minima of the potential P(u), and also continuum variants of the breather solutions. Analytical waveforms are available via the integrable theory for both kinks and breathers in the continuum sine-Gordon equation (see, for example, [8]). Kink solutions exist for the continuum ϕ^4 model as well, although that equation is not integrable [4, 22] and

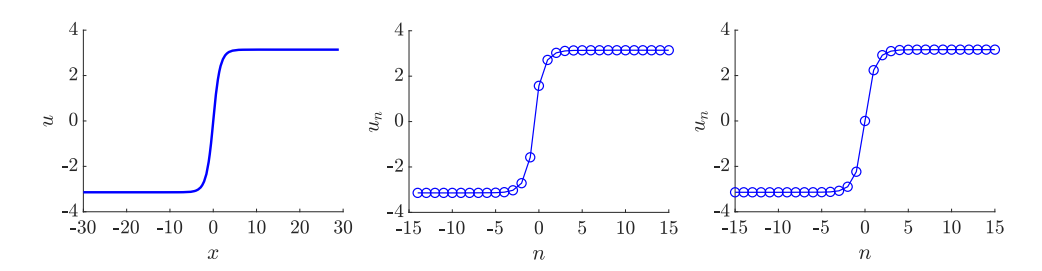


Figure 1. Kink solution to the sine-Gordon equation (left). Intersite spectrally stable (center) and onsite spectrally unstable (right) kinks of the discrete sine-Gordon equation for d = 0.5 and n = 60 lattice points.

the same is generically true for Klein–Gordon models with multiple degenerate energy minima. Regular breather waveforms do not exist in the continuum ϕ^4 model (and generically in continuum Klein–Gordon settings aside from the integrable sine-Gordon case) as is known from the work of [23].

When we move from the continuum realm to the discrete, there are two distinct kink solutions: intersite kinks (figure 1, which connect two adjacent minima of the potential P(u) directly, and onsite kinks (figure 1, right panel), which connect these states via a local maximum of P(u) which lies between the two minima [24]. This is similar to the discrete nonlinear Schrödinger equation (DNLS), where there is both a site-centered and an intersite-centered (pulse) soliton solution [25]. Corresponding to each kink solution is an antikink solution which connects the two equilbria in the opposite order. By reversibility, if k(n) is a kink solution, then k(-n) is an antikink. We will be concerned only with static kink solutions here, although we note that there has been much interest in both moving kinks [26–28] and breather solutions (see, for example, [4] as well as [29, 30] for results on multi-site breathers) in discrete Klein–Gordon lattices.

In this paper, we look at multi-kinks, which are coherent structures resembling a sequence of alternating kinks and antikinks spliced together end-to-end. The study of complex coherent structures formed by joining multiple copies of a simpler coherent structure has a rich mathematical history (see [31], and the references therein). In [31], for example, the existence and stability of multi-pulse solutions to semilinear parabolic equations, such as reaction diffusion equations, is determined using Lin's method [32, 33], an implementation of the Lyapunov–Schmidt reduction. This method constructs multi-pulses by splicing together multiple, well-separated copies of a single pulse using small remainder functions, and it is also used to reduce the PDE eigenvalue problem to a matrix eigenvalue problem. These techniques have been recently extended to Hamiltonian lattice systems, including DNLS [34]. In the case of DNLS, multi-pulse solutions exist on the lattice which do not exist in the continuum equation (although multi-pulses do exist in higher order NLS models [35]).

For the discrete Klein–Gordon equation, we follow a similar approach to [34] and use a discrete adaptation of Lin's method [36] to construct multi-kinks from a sequence of well-separated kinks and antikinks. As with multi-pulses in DNLS, these multi-kinks do not exist in the continuum equation. Indeed, it is the so-called Peierls–Nabarro barrier [24], the local effective potential due to discreteness, that makes such configurations possible. Otherwise, similarly to the DNLS case [37], the structures would purely interact exponentially through their tails, being unable to form stationary patterns involving multiple waves. We also use Lin's method to reduce the spectral problem to a matrix equation. The most notable difference here is that the system on the lattice is no longer translation invariant, thus there is not an

eigenvalue at 0. Instead of locating eigenvalues in a small ball around the origin, this method locates eigenvalues of the multi-kink in the neighborhood of each eigenvalue of the primary kink. In particular, this means that there will be a different matrix reduction corresponding to each eigenvalue of the primary kink; computing each of these matrices requires knowing (or computing numerically) the point spectrum and the corresponding eigenfunctions of the primary kink. We show that for an *m*-component multi-kink, there are *m* eigenvalues in the point spectrum near each eigenvalue of the primary kink. We obtain analytic expressions for these eigenvalues in terms of the tails of the eigenfunctions of the primary kink, in a similar fashion to the expressions for DNLS which depend on the tails of the primary pulse [34]. These expressions are in good agreement with numerical computations for intermediate values of the coupling parameter *d*. Finally, we perform timestepping experiments on perturbations of the primary kink and multi-kinks to illustrate the role of the point spectrum and its corresponding eigenfunctions in explaining the evolution of these perturbations. We believe that this offers a systematic understanding of such multiwave patterns, based on the existence and stability properties of the corresponding building block, namely the single kink (or antikink).

This paper is organized as follows. In section 2, we present the mathematical background for the discrete Klein–Gordon equation, together with a reformulation of the existence and eigenvalue problems using a spatial dynamics approach. The main results concerning the existence and spectrum of multi-kinks are then given in section 3; the proofs of these results are deferred to the end of the paper. In section 4, we present numerical results which corroborate the main theorems, as well as results of timestepping simulations. The proofs of theorems 1 and 2 are given as appendices following a brief concluding section.

2. Mathematical background

We will consider the discrete Klein–Gordon equation with onsite nonlinearity f(u)

$$\ddot{u}_n = d(\Delta_2 u)_n - f(u_n),\tag{4}$$

where $(\Delta_2 u)_n = u_{n+1} - 2u_n + u_{n-1}$ is the discrete second difference operator, and f(u) = P'(u) for a smooth potential function P(u). The nonlinearity f has the following three properties:

- (a) f(u) is an odd function with f'(0) < 0. This implies that f(0) = 0, so 0 is an equilibrium of (4).
- (b) There is a pair of nonzero equilibria $\pm u^*$ with $f(\pm u^*) = 0$ and $f'(u^*) = f'(-u^*) > 0$.
- (c) There are no other equilibria in $[-u^*, u^*]$.

Important versions include the discrete sine-Gordon equation, where $f(u) = -\sin(u)$ and $P(u) = 1 + \cos(u)$, and the ϕ^4 model, where $f(u) = -u(1 - u^2)$ and $P(u) = \frac{1}{4}(1 - u^2)^2$. We note that the discrete sine-Gordon equation is typically written with the nonlinearity $f(u) = \sin u$, in which case the pair of stable equilibria in (b) are at 0 and 2π , and the unstable one between them is at π . This is identical to the situation considered here except for a shift of u_n by $-\pi$. Choosing f to have odd symmetry greatly simplifies the analysis, and allows the result to apply to both the discrete sine-Gordon equation and the ϕ^4 model. Equation (4) is Hamiltonian, with energy given by [22]

$$\mathcal{H}(u) = \sum_{n = -\infty}^{\infty} \left(\frac{1}{2} (\dot{u}_n)^2 + \frac{d}{2} (u_{n+1} - u_n)^2 + P(u_n) \right). \tag{5}$$

The equilibrium solutions we will study are standing waves which satisfy

$$d(\Delta_2 u)_n - f(u_n) = 0. ag{6}$$

Linearization about an equilibrium solution u_n yields the eigenvalue problem

$$d(\Delta_2 v)_n - f'(u_n)v_n = \lambda^2 v_n. \tag{7}$$

Letting $\omega = \lambda^2$, we obtain the eigenvalue problem for ω

$$d(\Delta_2 v)_n - f'(u_n)v_n = \omega v_n. \tag{8}$$

The eigenvalues are given by $\lambda = \pm \sqrt{\omega}$. Equation (8) has the form of an infinite dimensional matrix problem [38]. Since that matrix is real and symmetric, the linear operator defined by the lhs of (8) is self-adjoint, thus ω must be real. This implies that the eigenvalues λ must be either real or purely imaginary pairs. In particular, spectral instabilities can only develop when a pair of eigenvalues passes through the origin [38].

Using a spatial dynamics approach as in [34], let u_n be an equilibrium solution to (6), and let $U(n) = (u(n), \tilde{u}(n)) = (u_n, u_{n-1})$. Then equation (6) is equivalent to the lattice dynamical system in \mathbb{R}^2

$$U(n+1) = F(U(n)), \tag{9}$$

where

$$F\begin{pmatrix} u\\ \tilde{u} \end{pmatrix} = \begin{pmatrix} 2u - \tilde{u} + \frac{1}{d}f(u)\\ u \end{pmatrix}.$$

Equation (9) has three fixed points of interest at 0 and $S^{\pm} = (\pm u^*, \pm u^*)^T$. (It may in fact have more, depending on the specific form of f(u); this is the case for the discrete sine-Gordon equation.) Linearizing about the fixed points S^{\pm} , we obtain the matrix

$$DF(S^{\pm}) = \begin{pmatrix} 2 + \frac{1}{d}f'(\pm u^*) & -1 \\ 1 & 0 \end{pmatrix}.$$

Since $f'(\pm u^*) > 0$, this has a pair of eigenvalues $\{r, 1/r\}$ with r > 0, where

$$r = \frac{1}{2d} \left(f'(u^*) + 2d + \sqrt{f'(u^*)(f'(u^*) + 4d)} \right). \tag{10}$$

Thus S^{\pm} are hyperbolic saddle equilibria of the lattice dynamical system (9). The origin is a nonhyperbolic equilibrium which has a pair of eigenvalues on the unit circle in the complex plane. We take the existence of a stable, symmetric kink (stationary front) as a hypothesis. From the spatial dynamics perspective, this kink solution is a heteroclinic orbit connecting the saddle at S^{-} to the saddle at S^{+} .

Hypothesis 1. There exists a kink solution $K(n) = (k(n), \tilde{k}(n))$ to (9) which connects the unstable manifold $W^{\rm u}(-u^*, -u^*)$ and the stable manifold $W^{\rm s}(u^*, u^*)$. These manifolds intersect transversely in \mathbb{R}^2 . The kink has the odd symmetry k(-n) = -k(n-1). Finally, = the kink K(n) is a minimizer of the t-independent energy functional

$$h[u] = \sum_{n = -\infty}^{\infty} \left(\frac{d}{2} (u_{n+1} - u_n)^2 + P(u_n) \right)$$
 (11)

among the class of heteroclinic connections between S^- and S^+ .

Remark 1. The kink k(n) from hypothesis 1 has the odd symmetry k(-n) = -k(n-1), and is known as an intersite kink, since it does not involve the equilibrium at 0. For the sine-Gordon equation, an intersite kink at the anti-continuum (AC) limit d = 0 is given by $(\dots, -\pi, -\pi, \pi, \pi, \dots)$. By contrast, an onsite kink, which has the odd symmetry k(-n) = -k(n), involves the equilibrium at 0. For the sine-Gordon equation, an onsite kink at the AC limit is $(\dots, -\pi, -\pi, 0, \pi, \pi, \dots)$.

Since K(n) is a minimizer of the energy functional (11), the spectrum of K(n) lies on the imaginary axis [22, section 2.1.6]. For specific nonlinearities f(u), including those associated with the discrete sine-Gordon equation and the ϕ^4 model, the existence of a symmetric, intersite kink which is a minimizer of (11) is known (see [8, 22] and references therein). On the other hand, the onsite kink will in general be unstable. For the sine-Gordon equation, for example, the onsite kink has a pair of real eigenvalues $\pm \lambda$ and is thus unstable [39, theorem 4.4]. In addition, the onsite kink can be shown to be unstable for the sine-Gordon equation when d < 1/4 and the ϕ^4 model when d < 1/2 using Gerschgorin's theorem [8]. While the former result is an asymptotic one, valid in the vicinity of the continuum limit, the latter is a rigorous one, but *only* valid for the above-mentioned interval of d in the vicinity of the AC limit of d = 0. Hence, the two results are complementary to each other. Since f(u) is an odd function, if u_n is a solution to (6), so is $-u_n$. Thus for every kink solution K(n) to (9) there is a corresponding antikink solution $\tilde{K}(n) = -K(n)$.

The spectrum of the primary kink solution $K(n) = (k(n), \tilde{k}(n))$ can be decomposed into two disjoint sets: the point spectrum consists of isolated eigenvalues for which the corresponding eigenfunction is in $\ell^2(\mathbb{Z})$, and the continuous spectrum which consists of bounded, oscillatory modes. Following [22], the continuous spectrum depends only on the background state of the system and consists of the two symmetric intervals on the imaginary axis

$$\sigma_{\text{cont}} = \pm i \left[\sqrt{f'(u^*)}, \sqrt{f'(u^*) + 4d} \right]. \tag{12}$$

In particular, there is a gap in the continuous spectrum i $\left(-\sqrt{f'(u^*)}, \sqrt{f'(u^*)}\right)$ which contains the origin. The continuous spectrum will be the same for the linearization about any equilibrium solution involving the asymptotics of $u \to \pm u^*$.

The continuum Klein–Gordon equation $u_{tt} = u_{xx} - f(u)$ has an eigenvalue at 0 due to translation invariance which is referred to as the Goldstone mode. Since the discrete Klein–Gordon equation does not possess any continuous symmetries, there will be no eigenvalues at the origin. Instead, there will be a symmetric pair of eigenvalues, which is either real or purely imaginary. For the intersite kink we are considering, this pair will be imaginary since the entire spectrum is imaginary (it will be real for the onsite kink). This pair of eigenvalues is often termed Goldstone modes by extension of the Goldstone mode of the continuum equation, since these eigenvalues approach the origin as the discrete equation approaches the continuum limit, i.e. $d \to \infty$. For specific nonlinearities f(u) and certain values of the coupling parameter d, there may be additional eigenvalues, known as internal modes, which lie between the bands of the continuous spectrum. For the kinks which are minimizers of (11), these will also be purely imaginary. (See [22, 40] for a discussion of the spectrum of the kink solution, including the internal modes, for the discrete sine-Gordon equation and the ϕ^4 model.) We make the additional hypothesis that all point spectrum for the primary kink K(n) lies in the continuous spectrum gap.

Hypothesis 2. $|\lambda| < \sqrt{f'(u^*)}$ for all eigenvalues (point spectrum) λ of the primary kink K(n).

3. Multi-kinks

We can construct multi-kink solutions by joining together an alternating sequence of kinks and antikinks in an end-to-end fashion. By the symmetry of f(u), u_n is an equilibrium solution if and only if $-u_n$ is, thus we can always without loss of generality begin with a kink solution. We will characterize a multi-kink in the following way. Let m > 1 be the total number of kinks and antikinks. Let N_i (i = 1, ..., m - 1) be the distances (in lattice points) between consecutive kinks/antikinks. (As a mark of the position of the center of the kinks/antikinks, we use the position of the corresponding zero-crossing). We seek a solution which can be written piecewise in the form

$$U_{i}^{-}(n) = c_{i}K(n) + \tilde{U}_{i}^{-}(n) \qquad n \in [-N_{i-1}^{-}, 0] \quad i = 1, \dots, m$$

$$U_{i}^{+}(n) = c_{i}K(n) + \tilde{U}_{i}^{+}(n) \qquad n \in [0, N_{i}^{+}] \qquad i = 1, \dots, m,$$
(13)

where $c_i = (-1)^{i+1}$, $N_i^+ = \lfloor \frac{N_i}{2} \rfloor$, $N_i^- = N_i - N_i^+$, and $N_0^- = N_m^+ = \infty$. We also define

$$N = \frac{1}{2}\min\{N_i\}\tag{14}$$

as a characteristic distance, which will be used in the estimates of the remainder terms in (16). The individual pieces $U_i^{\pm}(n)$ are joined together end-to-end as in [31, 34, 36] to create the multi-kink solution U(n), which can be written in piecewise form as

$$U(n) = \begin{cases} U_i^- \left(n - \sum_{j=1}^{i-1} N_j \right) & \sum_{j=1}^{i-1} N_j - N_{i-1}^- + 1 \leqslant n \leqslant \sum_{j=1}^{i-1} N_j \\ U_i^+ \left(n - \sum_{j=1}^{i-1} N_j \right) & \sum_{j=1}^{i-1} N_j + 1 \leqslant n \leqslant \sum_{j=1}^{i-1} N_j + N_i^+ \end{cases}$$
 $i = 1, \dots, m,$ (15)

where we define $\sum_{j=1}^{0} N_j = 0$. Since we are taking $N_0^- = N_m^+ = \infty$, this formula makes sense for the two end pieces $U_1^-(n)$ and $U_m^+(n)$. The functions $\tilde{K}_i^{\pm}(n)$ in (13) are remainder terms, which will be small. We then have the following existence theorem. The proof is deferred until appendix A.

Theorem 1. Assume hypothesis 1. Then there exists a positive integer N_0 with the following property. For all m > 1 and distances $N_i \ge N_0$, there exists a unique solution U(n) which is composed of m alternating kinks and antikinks and can be written piecewise in the form (13). For the remainder terms $\tilde{U}_{i}^{\pm}(n)$, we have the estimates

$$\|\tilde{U}_{i}^{\pm}\| \leqslant Cr^{-N}$$

$$|\tilde{U}_{i}^{-}(n)| \leqslant Cr^{-N_{i-1}^{-}}r^{-(N_{i-1}^{-}+n)} \qquad n = 2, \dots, m$$

$$|\tilde{U}_{i}^{+}(n)| \leqslant Cr^{-N_{i}^{+}}r^{-(N_{i}^{+}-n)} \qquad n = 1, \dots, m-1$$

$$|\tilde{U}_{1}^{-}(n)| \leqslant Cr^{-2N}r^{n}$$

$$|\tilde{U}_{m}^{+}(n)| \leqslant Cr^{-2N}r^{-n}.$$
(16)

Remark 2. For the sine-Gordon equation, equation (9) has saddle equilibria at $n\pi$ for all odd integers n. More general multi-kinks can be constructed comprising kinks and antikinks which link any adjacent saddle equilibria. A specific example is a double kink, where a kink connecting $-\pi$ to π is followed by a kink connecting π to 3π . The existence of these general multi-kinks is a straightforward adaptation of theorem 1.

To determine the eigenvalues of the linearization about a multi-kink, we again take a spatial dynamics approach. We rewrite (8) as a lattice dynamical system by taking $V(n) = (v(n), \tilde{v}(n)) = (v_n, v_{n-1})$. Then (8) is equivalent to the lattice dynamical system in \mathbb{R}^2

$$V(n+1) = DF(U(n))V(n) + \omega BV(n), \tag{17}$$

where

$$B = \frac{1}{d} \begin{pmatrix} 1 & 0 \\ 0 & 0 \end{pmatrix}.$$

For the primary kink $K(n) = (k_n, \tilde{k}_n)$, let $v_0(n)$ be an eigenfunction with corresponding eigenvalue λ_0 , let $\omega_0 = \lambda_0^2$, and let $V_0(n) = (v_0(n), \tilde{v}_0(n)) = (v_0(n), v_0(n-1))$. Then $V_0(n)$ solves the equation

$$V_0(n+1) = DF(K(n))V_0(n) + \omega_0 BV_0(n), \tag{18}$$

which we rewrite as

$$V_0(n+1) = A(n; \omega_0)V_0(n), \tag{19}$$

where

$$A(n;\omega) = DF(K(n))V_0(n) + \omega B. \tag{20}$$

By the stable manifold theorem,

$$|A(n;\omega_0) - A_0| \leqslant Cr^{-|n|},\tag{21}$$

where A_0 is the constant matrix

$$A_0 = DF(S^+) + \omega_0 B. \tag{22}$$

 A_0 has eigenvalues $\{r_0, 1/r_0\}$, where

$$r_0 = \frac{1}{2d} \left(f'(u^*) + \omega_0 + 2d + \sqrt{(f'(u^*) + \omega_0)(f'(u^*) + \omega_0 + 4d)} \right). \tag{23}$$

Since λ_0 is on the imaginary axis by hypothesis 1, $\omega_0 < 0$, thus it follows from hypothesis 2 that A_0 is hyperbolic. It also follows from hypothesis 2 that $1 < r_0 < r$, thus the eigenfunctions decay to 0 slower than the kink solution decays to the equilibria at $\pm S$.

For a multi-kink composed of m components, each eigenvalue of the primary kink K(n) will split into m eigenvalues. The following theorem locates these eigenvalues for the multi-kink U(n). The proof is deferred until appendix B.

Theorem 2. Assume hypothesis 1 and 2. Let U(n) be an m-component multi-kink constructed as in theorem 1 with distances N_i , and let $N = \frac{1}{2} \min\{N_1, \ldots, N_{m-1}\}$. Let $\pm \lambda_0$ be

a pair of purely imaginary eigenvalues for the primary kink with corresponding eigenfunction $V_0(n)$, and let $\omega_0 = \lambda_0^2$. Then for N sufficiently large, the multi-kink U(n) has m pairs of imaginary eigenvalues $\{\pm \lambda_0^1, \ldots, \pm \lambda_0^m\}$ which are close to $\pm \lambda_0$ and are given by

$$\lambda_0^j = \sqrt{\omega_j}, \quad \omega_j = \lambda_0^2 + \frac{d\mu_j}{M} + \mathcal{O}(r_0^{-3N}) \quad j = 1, \dots, m,$$
 (24)

where r_0 is defined in (23), $\{\mu_1, \ldots, \mu_m\}$ are the real, distinct eigenvalues of the symmetric, tridiagonal matrix

$$A = \begin{pmatrix} 0 & a_1 & & & \\ a_1 & 0 & a_2 & & & \\ & a_2 & 0 & a_3 & & \\ & & \ddots & \ddots & & \\ & & & a_{m-1} & 0 \end{pmatrix}, \tag{25}$$

with

$$a_i = v_0(N_i^+)v_0(-N_i^- - 1) - v_0(N_i^+ - 1)v_0(-N_i^-),$$
(26)

and M is the Melnikov sum

$$M = \sum_{n = -\infty}^{\infty} v_0(n)^2 = ||v_0||_{\ell^2}.$$
 (27)

Remark 3. The results of theorem 2 hold as well for multi-kinks constructed using the unstable, onsite kink. In that case, the multi-kink U(n) would have m pairs of real eigenvalues close to each real eigenvalue pair $\pm \lambda_0$ of the onsite kink.

Remark 4. The estimates in theorem 2, and in particular the matrix (25), require knowledge of both the eigenvalue λ_0 of the primary kink and its corresponding eigenfunction $v_0(n)$. The matrix A will be different for each eigenvalue λ_0 of the primary kink. In particular, note that the decay rate of the remainder term in (24) depends on λ_0 via r_0 .

For m = 2 and m = 3, we can compute the eigenvalues of A exactly.

Corollary 1. For m = 2,

$$\omega_1 = \lambda_0^2 + \frac{d}{M}a_1 + \mathcal{O}(r_0^{-3N})$$

$$\omega_2 = \lambda_0^2 - \frac{d}{M}a_1 + \mathcal{O}(r_0^{-3N}).$$

For m=3,

$$\begin{split} \omega_1 &= \lambda_0^2 + \mathcal{O}(r_0^{-3N}) \\ \omega_2 &= \lambda_0^2 + \frac{d}{M} \sqrt{a_1^2 + a_2^2} + \mathcal{O}(r_0^{-3N}) \\ \omega_3 &= \lambda_0^2 - \frac{d}{M} \sqrt{a_1^2 + a_2^2} + \mathcal{O}(r_0^{-3N}). \end{split}$$

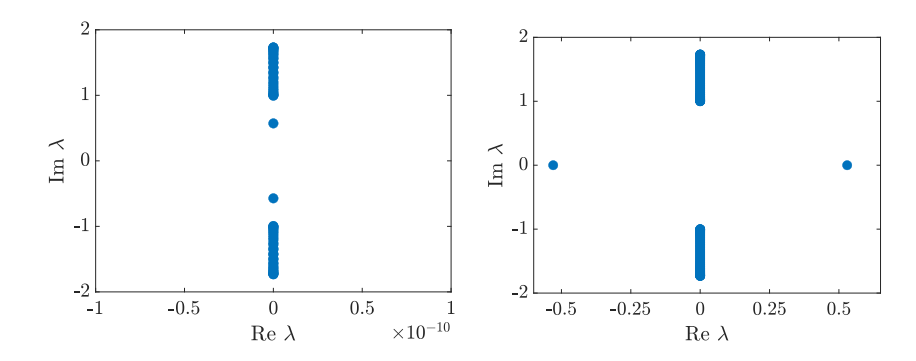


Figure 2. Spectrum of the primary spectrally stable intersite kink (right) and of the spectrally unstable onsite kink (left) for the discrete sine-Gordon equation with d = 0.50.

Remark 5. Theorem 2 can be easily adapted to the case of general multi-kinks in the discrete sine-Gordon equation (see remark 2). The matrix (25) will have a similar form. The spectrum of all general multi-kinks will be purely imaginary as long as the multi-kink comprises only stable, intersite kinks.

4. Numerical results

The results we present here are from the discrete sine-Gordon equation $\ddot{u}_n = d(\Delta_2 u)_n + \sin(u_n)$. We start by constructing the primary, intersite kink solution k_n by using MATLAB for numerical parameter continuation from the AC limit (d=0) in the coupling parameter d, starting with the solution $(\ldots, -\pi, -\pi, \pi, \pi, \ldots)$ (figure 1, center). (The right panel of figure 1 shows the onsite kink). We then compute the spectrum of the linearization about the primary kink k_n using MATLAB's eig function (figure 2). As expected [22, 38], the spectrum of the intersite kink is imaginary, whereas the spectrum of the onsite kink contains a symmetric pair of real eigenvalues, thus it is unstable. Most of the remaining numerical results will only concern stable, intersite kinks.

The continuous spectrum lies within the interval given by (12), and the pair of Goldstone mode eigenvalues is clearly visible in the continuous spectrum gap. For approximately d > 0.265, there is an additional internal mode eigenvalue for the intersite kink (not discernible in the left panel of figure 2), which is known as an edge mode since it arises from the continuous spectrum (see [22, section 2.2], noting that we are using d in place of d^2 in that paper.) The eigenfunctions corresponding to the Goldstone mode and the edge mode are shown on the left and middle panels of figure 3. The semilog plot on the right panel shows the exponential decay of the primary kink to π and the eigenfunctions to 0 as the lattice site index n increases. These decay rates are predicted to be $r^{-|n|}$ for the primary kink, and $r_0^{-|n|}$ for the eigenfunctions, where r is given by (10) and r_0 (which depends on the eigenvalue) is given by (23). The decay rates computed from the least squares linear regression lines have a relative error of order 10^{-4} for the kink and the Goldstone mode and a relative error of 10^{-2} for the edge mode.

We construct a kink-antikink (figure 5, middle panel) by parameter continuation in the coupling parameter d from the AC limit using the software package AUTO. As an initial condition, we use a kink-antikink composed of two intersite kinks, which at the AC limit has the form $(\ldots, -\pi, -\pi, \pi, \pi, \ldots, \pi, -\pi, -\pi, \ldots)$, where there are N_1 sites in the middle of the

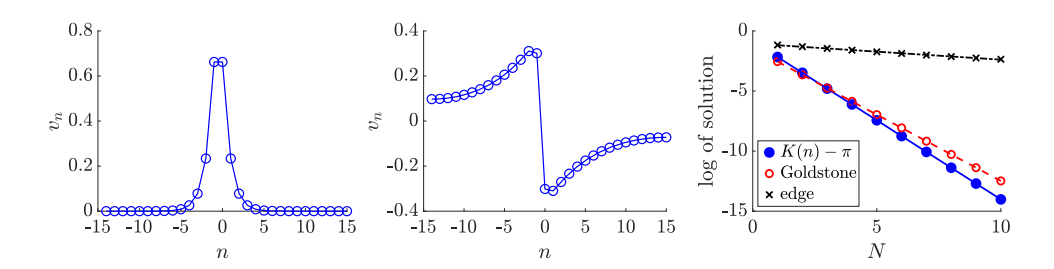


Figure 3. Goldstone mode eigenfunction ($\lambda=\pm 0.5718$ i, left) and edge mode eigenfunction ($\lambda=\pm 0.9941$ i, center). Semilog plot of decay of primary kink to $\pm \pi$ and decay of Goldstone and edge modes to 0 (right). Lines are least-squares linear regressions. d=0.50 and n=60 lattice points.

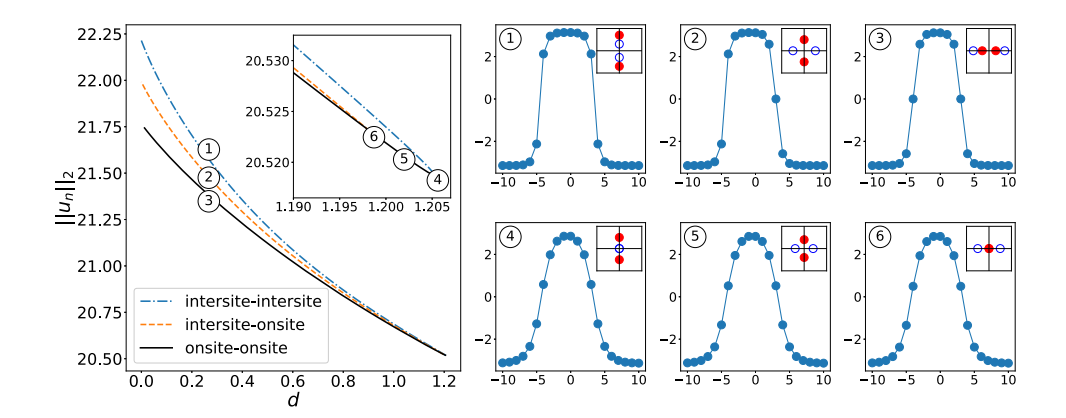


Figure 4. The left panel shows the bifurcation diagram for a kink–antikink waveform with $N_1 = 8$, plotting the ℓ^2 norm of solution versus coupling parameter d. The three branches shown correspond intersite–intersite, intersite–onsite, and onsite–onsite kink–antikinks. The inset details the intersection points of the three branches. The right panel shows six example solutions, corresponding to the labeled points on the bifurcation diagram. The insets are cartoons of the Goldstone eigenvalues for these solutions; a single marker at the origin represents a double eigenvalue at 0.

solution which take the value π . The bifurcation diagram for the parameter continuation is shown in figure 4. Notably, there is a turning point at a critical value d_0 (label 4 in the inset), where the kink–antikink does not exist for $d > d_0$. Indeed, this is natural to expect as, in the continuum limit of the model, the attractive interaction between the kink and antikink [41] cannot be countered by discreteness and the associated Peierls–Nabarro barrier, and hence such a bound, stationary state cannot exist. The top branch of the bifurcation diagram in figure 5 is a kink–antikink comprising two intersite kinks, and the bottom branch is a kink–antikink comprising two onsite kinks. However, a direct eigenvalue count illustrates that these branches cannot 'collide' with each other at a turning point (i.e., at a saddle-center bifurcation). This because the intersite kink state is stable, while the onsite one contains two unstable eigenvalue pairs. Hence, there must exist also an intermediate branch with one unstable eigenvalue pair. Indeed, such a middle branch exists, and is an asymmetric kink–antikink comprising one intersite kink and one onsite kink, which meets the bottom branch at a pitchfork bifurcation point (indeed, there are two realizations of the intersite–onsite kink which are mirror images of

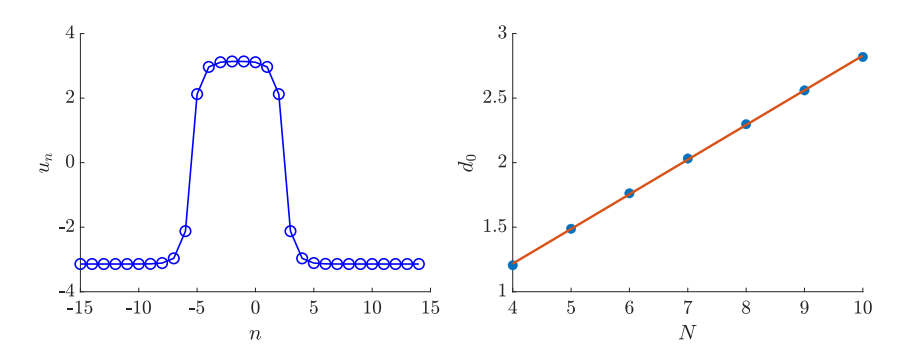


Figure 5. The left panel shows a kink–antikink solution with $N_1 = 8$ for d = 0.5. The right panel shows the turning point d_0 vs N for kink–antikink waveforms together with least squares linear regression line.

each other, as discussed in more detail below) at a value of d slightly smaller than d_0 . The center branch of the bifurcation diagram in figure 4 is composed of two branches: solutions on one branch are an intersite kink followed by an onsite antikink (label 2), and solutions on the other branch are an onsite kink followed by an intersite antikink (not shown in the figure). Solutions on these two branches are left-right mirror images of each other and have the same ℓ^2 norm at the same value of d. Insets in the right panel of figure 4 show the Goldstone eigenvalue pattern for the kink—antikink solutions. Pairs of Goldstone eigenvalues collide at the origin at the turning point and the pitchfork bifurcation points. First, the collision of the asymmetric intersite—onsite branch with the onsite—onsite one takes place: as a result of this pitchfork bifurcation, the asymmetric branch disappears, and the symmetric waveform emerging thereafter has only a single pair of unstable eigenvalues. Then, at the turning point, it collides in turn with the intersite—intersite branch, and the branches disappear past this critical point d_0 of the collision. The parameter continuation suggests a linear relationship between the critical value of the coupling parameter d_0 and the separation distance N, which is shown in the right panel of figure 5.

The spectrum of the kink-antikink is similarly computed (figure 6, left panel) using MATLAB's eig function. As predicted by theorem 2, each element of the point spectrum splits into two eigenvalues. The eigenfunctions corresponding to the split Goldstone modes resemble two copies of the Goldstone eigenfunction of the primary kink, spliced together both in-phase and out-of-phase (figure 6, center panel). A similar phenomenon occurs with the split edge mode eigenfunctions (figure 6, right panel).

We can compare the eigenvalues obtained from numerical computation with those predicted by corollary 1. The left panel of figure 7 plots the log of the relative error $|\lambda_{\text{true}} - \lambda_{\text{predicted}}|/|\lambda_{\text{true}}|$ of the two Goldstone eigenvalues vs the separation distance N; the value for λ computed with MATLAB from the linearization around the numerically computed kink–antikink solution is used as the true value of λ . The slope of the least square linear regression line suggests that this error is order $\mathcal{O}(r_0^{-2N})$. The right panel of figure 7 plots the log of the relative error of the two Goldstone eigenvalues vs the coupling parameter d. For intermediate values of d, the relative error is less than 10^{-3} . The error is a minimum for approximately d=0.2, and increases with increasing d and as the continuum limit is approached. (See [34, figure 4] for a similar phenomenon which occurs in the error plot for eigenvalues associated with double pulses in DNLS.) Since the results of the theorem 2 are not uniform in d, i.e. they

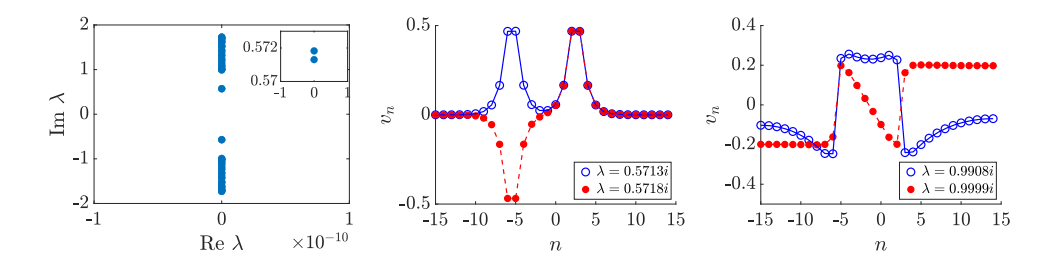


Figure 6. The left panel shows the spectrum of the kink–antikink, with an inset showing splitting of the Goldstone mode. The edge mode is also split (not shown). The center panel shows the eigenfunctions corresponding to the split Goldstone modes. The right panel shows the eigenfunctions corresponding to the split edge modes. d = 0.5, N = 4.

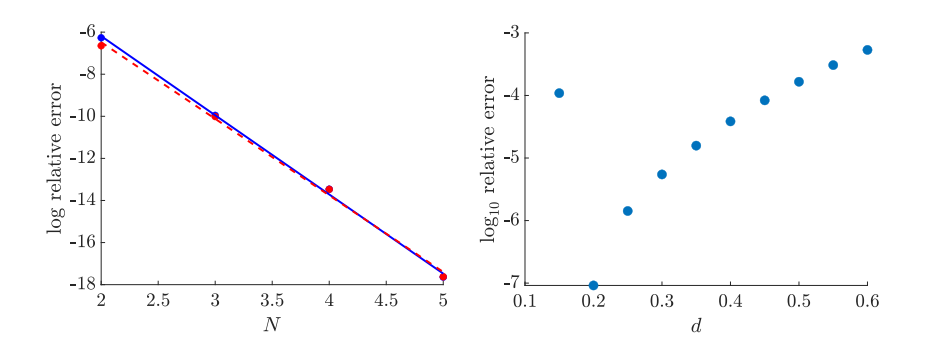


Figure 7. The left panel shows the log of the relative error in eigenvalue computation vs N for the two Goldstone eigenvalues for the kink–antikink with d = 0.25 together with least square linear regression lines. Blue dots and solid line denote one Goldstone eigenvalue, while red dots and dashed line the other Goldstone eigenvalue. The right panel shows \log_{10} of the relative error in the eigenvalue computation vs d for the two Goldstone eigenvalues for a kink–antikink waveform with N = 4.

hold for sufficiently large N once d has been chosen, we indeed expect a growth of the relative error for large d.

We can obtain similar results for higher order multi-kinks. An example of a three-component multi-kink is shown in the left panel of figure 8. We can again compare the eigenvalues obtained from numerical computation with those predicted by corollary 1. The right panel of figure 8 shows the relative error of the eigenvalue computations for the three Goldstone eigenvalues. One can again observe the particularly good agreement of the theory and the computation, especially so for larger values of N.

In addition, for the sine-Gordon equation, we can have generalized multi-kink solutions, in which each kink or antikink in the sequence connects two adjacent saddle equilbria (see remark 2). An example of a kink-kink is shown in figure 9. The spectrum is almost identical to that of the kink-antikink with the same parameters in figure 6.

Finally, we perform timestepping simulations of the multikink states. The topic of the evolution of a single (primary) kink was touched upon in the work of [22], where dynamical evolution experiments were performed in the case of a single kink with the Goldstone and/or edge modes excited. It was found that a mechanism of resonance of the point spectrum mode harmonics (i.e., 2λ , 3λ etc, where λ is the Goldstone or edge eigenvalue) with the continuous

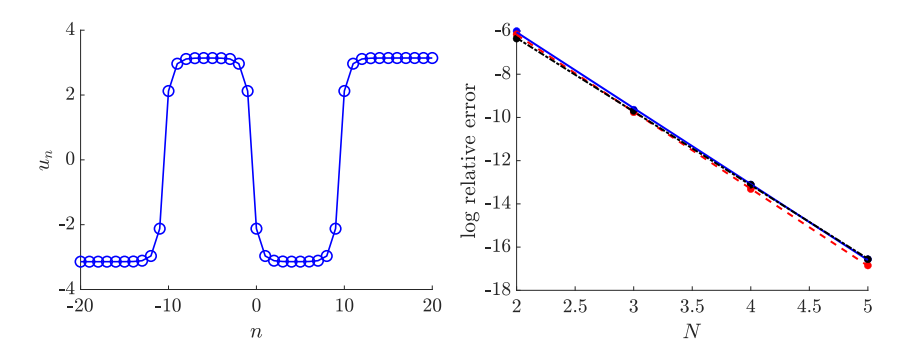


Figure 8. The left panel shows a three-component multi-kink (kink-antikink-kink) with $N_1 = N_2 = 8$ and d = 0.25. The right panel shows the log of the relative error in eigenvalue computation vs N for the three Goldstone eigenvalues of three-wave multi-kink with $N_1 = N_2 = 2N$ and d = 0.25. The lines are least square linear regression fits. Each line among the 3 very proximal solid, dashed and dash-dotted lines corresponds to one of the three Goldstone eigenvalues.

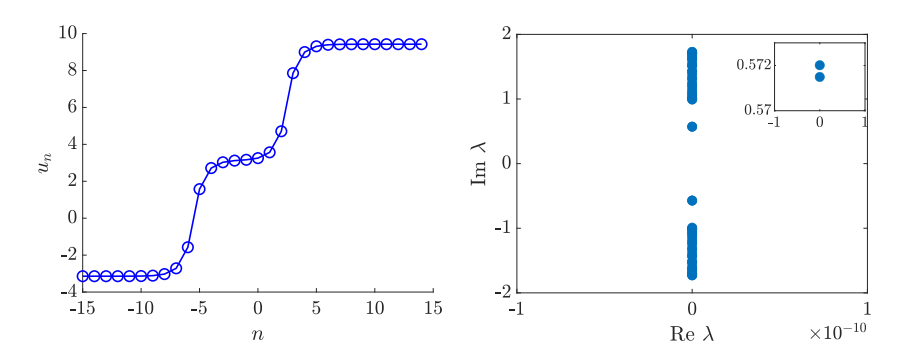


Figure 9. The left panel shows a kink–kink solution with $N_1 = 8$. The right panel shows the spectrum of the kink–kink waveform, with the inset showing splitting of Goldstone mode. The edge mode is also similarly split (not shown). d = 0.25.

spectrum led to nonlinearity-induced power law decay of relevant mode amplitudes. Here, we instead focus on the evolution of the central nodes of the kinks (e.g. nodes -1 and 0 for a kink located at the origin) for the realm of multi-wave, kink-antikink structures. For a timestepping scheme, since the spatial component is already discretized, we use a symplectic and symmetric implicit Runge-Kutta method [42], as suggested in [43, section 2.5], to preserve the symplectic structure of the Hamiltonian equation (1). Specifically, we use the MATLAB implementation of the <code>irk2</code> scheme of order 12 from [44]. For boundary conditions, we use the discrete analogue of Neumann boundary conditions.

For a kink–antikink constructed from two intersite kinks, the pair of Goldstone mode eigenfunctions suggests that there will be two corresponding normal modes of oscillations for the central nodes of the two kinks: an in-phase mode and an out-of-phase mode. These can be seen in the left and right columns of figure 10. In addition, we plot the energy of the solution H(u(n, t)) as t evolves (figure 10, bottom row). The relative deviation of the energy from its initial value is less than 10^{-15} over the time interval of the simulation. There will similarly be

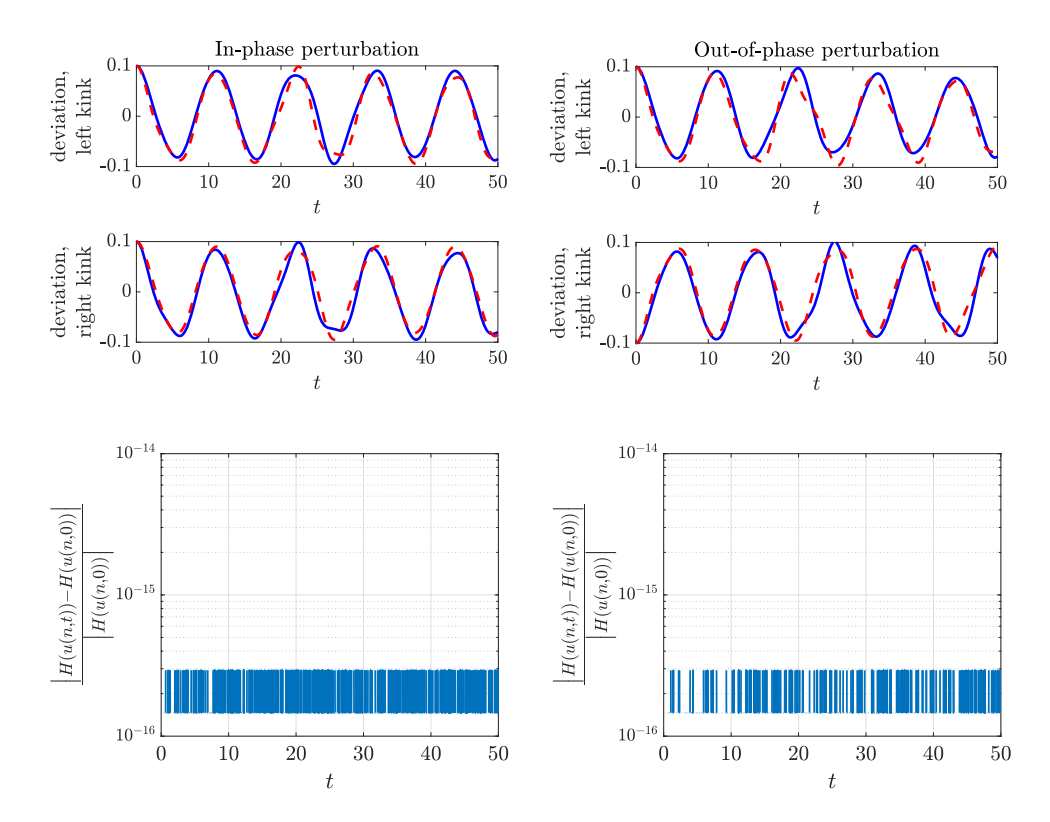


Figure 10. Timestepping of perturbations for a kink-antikink solution. The left column shows an in-phase perturbation, where the central nodes of both kinks are perturbed by 0.1 in the same direction. The right column shows an out-of-phase perturbation, where the central nodes of the left kink are perturbed by 0.1, and the central nodes of the right kink are perturbed by -0.1. First and second rows plot deviations from the stationary kink solution of the two central nodes for the left and right kinks (respectively). The third row is a semilog plot of the relative difference of the energy H(u(n,t)) from the starting energy H(u(n,0)). d=0.5, N=400 grid points, timestepping using symplectic and symmetric implicit Runge–Kutta method irk2 with step size 0.01.

two normal modes corresponding to the pair of edge mode eigenfunctions. These panels are representative of the possible in- and out-of-phase motion of the multiple coherent structures.

We can similarly construct a kink—antikink from two onsite kink structures (figure 11, top left). The spectrum corresponding to this solution is shown in the top right panel of figure 11, in which we see the split Goldstone modes on the real axis, confirming the instability of this bound state. The corresponding Goldstone eigenfunctions are shown in the bottom left panel of figure 11. Finally, we perform timestepping experiments for perturbations of this kink—antikink. If we perturb the two central nodes (both of which have values $u_n = 0$) by a small amount, the solution develops oscillatory behavior about the neutrally stable intersite kink—antikink (figure 11, bottom). The solution departs from the corresponding energy maximum and performs oscillations around the nearby energy minimum, namely the stable intersite kink—antikink state. The energy H(u(n, t)) is again very well conserved as t evolves (figure 11), with a relative deviation from its initial value of less than 10^{-15} . We note that for timestepping simulations on long time intervals, energy is very well conserved until boundary effects come

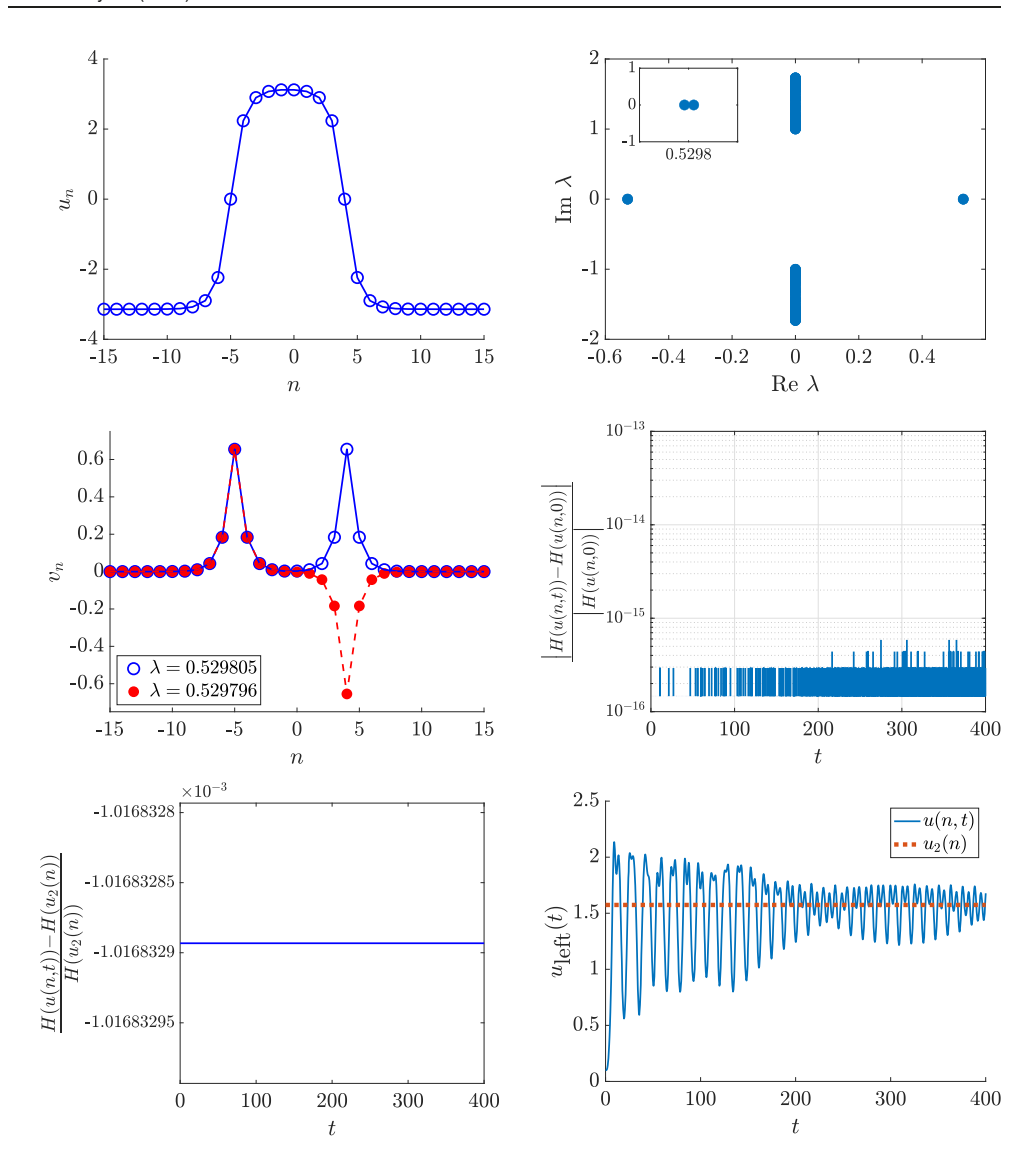


Figure 11. Kink–antikink solution constructed from two onsite kinks with $N_1 = 8$ (top left). Spectrum of onsite kink–antikink bearing two unstable near-identical Goldstone modes (top right); see also the inset discerning between the two modes. Eigenfunctions corresponding to the split Goldstone modes (middle left). Remaining plots show time evolution of perturbation u(n,t) of onsite kink–antikink; initial condition obtained by adding 0.1 to the two central nodes with $u_n = 0$, leading to the destabilization of the structure. Middle right is semilog plot of the relative difference of the energy H(u(n,t)) from the starting energy H(u(n,0)). Bottom left is energy difference between the perturbed onsite kink–antikink u(n,t) and the neutrally stable static intersite kink–antikink $u_2(n)$. Bottom right shows left central node of perturbed onsite kink–antikink u(n,t) (blue solid line) oscillating about left central node of static intersite kink–antikink $u_2(n)$ (horizontal, dotted orange line). N = 400 grid points, d = 0.5, timestepping using symplectic and symmetric implicit Runge–Kutta method irk2 with step size 0.01.

into play. For N = 200 and N = 400 grid points, these boundary effects occur at approximately t = 200 and t = 450, respectively; enlarging the spatial grid delays these boundary effects.

5. Conclusions and future challenges

In this paper, we used Lin's method to construct multi-kink solutions to the discrete Klein–Gordon equation by splicing together an alternating sequence of kink and antikink solutions with small amplitude remainders. These solutions exist as long as the distances between adjacent kinks and antikinks are sufficiently large. We then used Lin's method again to reduce the eigenvalue problem for multi-kinks to an effective, low-dimensional matrix eigenvalue equation. This matrix equation is different for each eigenvalue of the primary kink, and we find that for an *m*-component multi-kink, there are *m* eigenvalues near each eigenvalue of the primary kink. Most notably, if the spectrum of the primary kink is imaginary, the spectrum of a multi-kink constructed from these primary kinks can be shown through this explicit calculation to be imaginary as well. These eigenvalues can be computed numerically, and the result is in good agreement with the theory; this approach explicitly illustrates the spectral stability of these multi-soliton solutions.

Further avenues of research include exploring multi-kinks in other models. One such model is the Ablowitz–Ladik type discretization of the ϕ^4 model (AL- ϕ^4) [45]

$$\ddot{u}_n = \frac{1}{h^2} (\Delta_2 u)_n + 2u_n - u_n^2 (u_{n+1} + u_{n-1}), \tag{28}$$

which has an exact static kink solution $u_n = \tanh(an + \xi)$, where $a = \frac{1}{2}\cosh^{-1}[(1 + h^2)/(1 - h^2)]$ and ξ is arbitrary. Another is an alternative discretization of the sine-Gordon equation [46]

$$\ddot{u}_n \cos\left(\frac{u_{n+1} - u_{n-1}}{4}\right) = \frac{4}{h^2} \sin\left(\frac{u_{n+1} - 2u_n + u_{n-1}}{4}\right) - \sin\left(\frac{u_{n+1} + 2u_n + u_{n-1}}{4}\right),\tag{29}$$

which has an exact static kink solution

$$u_n(t) = 4 \arctan \left[\exp \left(kn - \frac{vt}{\sqrt{1 - v^2}} \right) \right],$$
 (30)

where k is defined implicitly by

$$\sinh\left(\frac{k}{2}\right) = \frac{1}{\sqrt{1 - v^2}} \frac{h}{\sqrt{4 - h^2}} - 1 < v < 1.$$
 (31)

Here, h is the lattice spacing, which is connected to our parameter d via $h=1/\sqrt{d}$, while v denotes the kink's speed. Although we do not expect these equations to have kink-antikink equilibrium solutions, since the stable and unstable manifolds of the two equilibria do not intersect transversely, we expect that a kink-antikink state will be an *approximate* equilibrium solution. We may then be able to explain the time evolution of the kink-antikink dynamics in terms of interactions between their exponentially decaying tails. In this context, it would be interesting to explore the potential mathematical relevance of the corresponding spectral calculation. While we have already mentioned that similar findings to the ones presented herein are applicable to other Klein-Gordon models, such as, e.g., the discrete ϕ^4 model, it would be of interest to study such ideas in more complex model variants such as the sine lattice

studied in the work of [47]. Generalizing such ideas to the context of higher-dimensional Klein–Gordon models where the kinks are typically also dynamically robust would be another direction of interest. We could also explore the time evolution using initial conditions which have the same asymptotics at $\pm\infty$ as a multi-kink. Finally, it remains open to explore whether similar techniques can be used to study multi-site breathers in discrete Klein–Gordon lattices.

Acknowledgments

This material is based upon work supported by the US National Science Foundation under the RTG Grant DMS-1840260 (RP and AA) and DMS-1809074 (PGK).

Appendix A. Proof of theorem 1

The proof is an adaptation of the proofs of theorems 1 and 3 in [34]. First, we rewrite the system as a fixed point problem. Expanding F(u) in a Taylor series about $c_iK(n)$, we get

$$F(U_i^{\pm}(n)) = F(c_i K(n) + \tilde{U}_i^{-}(n)) = DF(c_i K(n)) \tilde{U}_i^{\pm}(n) + G(\tilde{U}_i^{\pm}(n)), \tag{32}$$

where $G(\tilde{U}_i^{\pm}(n)) = \mathcal{O}(|\tilde{U}_i^{\pm}|^2)$ with G(0) = 0 and DG(0) = 0. Since f(u) is odd, f'(u) is even, thus $DF(c_iK(n)) = DF(K(n))$, and equation (32) becomes

$$F(U_i^{\pm}(n)) = DF(K(n))\tilde{U}_i^{\pm}(n) + G(\tilde{U}_i^{\pm}(n)). \tag{33}$$

Since the pieces U_i^{\pm} in the ansatz (13) must match at their endpoints, we obtain the following system of equations for the remainder functions \tilde{U}_i^{\pm}

$$U_i^{\pm}(n+1) = DF(K(n))U_i^{\pm}(n) + G(U_i^{\pm}(n))$$
(34)

$$\tilde{U}_{i}^{+}(N_{i}^{+}) - \tilde{U}_{i+1}^{-}(-N_{i}^{-}) = c_{i+1}K(-N_{i}^{-}) - c_{i}K(N_{i}^{+})$$
(35)

$$\tilde{U}_{i}^{+}(0) - \tilde{U}_{i}^{-}(0) = 0. \tag{36}$$

Let $\Phi(m, n)$ be the evolution operators for the linear difference equation

$$V(n+1) = DF(K(n))V(n).$$

By the stable manifold theorem, $|K(n) - S^+| \le Cr^{-|n|}$ for $n \ge 0$ and $|K(n) - S^-| \le Cr^{-|n|}$ for $n \le 0$, thus $|DF(K(n)) - DF(S^\pm)| \le Cr^{-|n|}$. Since S^\pm are hyperbolic fixed points, we can decompose the evolution operator $\Phi(m,n)$ in exponential dichotomies on \mathbb{Z}^\pm by [34, lemma 2]. The proof then follows that of [34, theorems 1 and 3]. Briefly, we write equation (34) in fixed-point form using the discrete variation of constants formula together with projections on the stable and unstable subspaces of the exponential dichotomy. As long as N is sufficiently large, we use the implicit function theorem to solve for the remainder functions \tilde{U}_i^\pm as well as the matching conditions (35) and (36). Since $W^u(S^-)$ and $W^s(S^+)$ intersect transversely, we have the decomposition $\mathbb{R}^2 = T_{K(0)}W^u(S^-) \oplus T_{K(0)}W^s(S^+)$, thus, as in the proof of [34, theorem 3], solving (36) does not involve jump conditions. The estimates (16) follow from the proof of [34, theorem 3] (see in particular [34, lemma 4]).

Appendix B. Proof of theorem 2

For the multi-kink solution U(n), we will take an ansatz which is a piecewise perturbation of $V_0(n)$. (This ansatz is suggested in [31, section 7]). Let

$$V_i^{\pm}(n) = s_i c_i V_0(n) + W_i^{\pm}(n), \tag{37}$$

where $s_i \in \mathbb{R}$, $s = (s_1, \dots, s_n)$, and $c_i = (-1)^{i+1}$. Substituting this into (17) and simplifying using (18), the eigenvalue problem becomes

$$W_{i}^{\pm}(n+1) = DF(K(n))W_{i}^{\pm}(n) + \omega_{0}BW_{i}^{\pm}(n) + [G_{i}^{\pm}(n) + (\omega - \omega_{0})B](s_{i}c_{i}V_{0}(n)W_{i}^{\pm}(n)),$$
(38)

where

$$G_i^{\pm}(n) = DF(U_i^{\pm}(n)) - DF(K(n)),$$
 (39)

and we used the fact that $DF(c_iK(n)) = DF(K(n))$ from the previous section. Using (20), we rewrite (38) as

$$W_i^{\pm}(n+1) = A(n;\omega_0)W_i^{\pm}(n) + [G_i^{\pm}(n) + (\omega - \omega_0)B](s_ic_iV_0(n) + W_i^{\pm}(n)). \tag{40}$$

In addition to solving (40), the eigenfunction must satisfy matching conditions at $n = \pm N_i$ and n = 0. Thus the system of equations we need to solve is

$$W_{i}^{\pm}(n+1) = A(n;\omega_{0})W_{i}^{\pm}(n) + [G_{i}^{\pm}(n) + (\omega - \omega_{0})B](s_{i}c_{i}V_{0}(n) + W_{i}^{\pm}(n))$$

$$W_{i}^{+}(N_{i}^{+}) - W_{i+1}^{-}(-N_{i}^{-}) = S_{i}s$$

$$W_{i}^{+}(0) - W_{i}^{-}(0) = 0,$$

$$(41)$$

where

$$S_{i}s = s_{i+1}c_{i+1}V_{0}(-N_{i}^{-}) - s_{i}c_{i}V_{0}(N_{i}^{+}).$$

$$(42)$$

Let $\Phi(m, n)$ be the evolution operator for the variational equation

$$V(n+1) = A(n; \omega_0)V(n). \tag{43}$$

Since we have the exponential decay (21), by [34, lemma 2], we can decompose the evolution operator $\Phi(m, n)$ in exponential dichotomies on \mathbb{Z}^{\pm} . In particular, we have the estimates

$$\begin{aligned} |\Phi_{+}^{s}(m,n)| &\leqslant C r_{0}^{-(m-n)} & 0 \leqslant n \leqslant m \\ |\Phi_{+}^{u}(m,n)| &\leqslant C r_{0}^{-(n-m)} & 0 \leqslant m \leqslant n \\ |\Phi_{-}^{s}(m,n)| &\leqslant C r_{0}^{-(m-n)} & n \leqslant m \leqslant 0 \\ |\Phi_{-}^{u}(m,n)| &\leqslant C r_{0}^{-(n-m)} & m \leqslant n \leqslant 0, \end{aligned}$$
(44)

for the evolution operator on the stable and unstable subspaces of the exponential dichotomy. Furthermore, letting $E^{s/u}$ be the stable and unstable eigenspaces of A_0 , and $P_0^{s/u}$ the corresponding eigenprojections, we have the decay rates

$$|P_{\pm}^{s/u}(n) - P_0^{s/u}| \leqslant Cr^{-|n|},$$
 (45)

where $P_{\pm}^{s/u}(n) = \Phi_{\pm}^{s/u}(n, n)$ are the stable and unstable projections for the exponential dichotomy. We note that the decay rates in (44) involve the eigenvalues for the matrix A_0 , whereas those from (45) come from (21).

The variational equation (43) has a bounded solution $V_0(n) = (v_0(n), v_0(n-1))$, and the adjoint variational equation

$$Z(n) = A(n; \omega_0)^* Z(n+1)$$
(46)

has a bounded solution

$$Z_0(n) = (-v_0(n-1), v_0(n)), \tag{47}$$

which is orthogonal to $Z_0(n)$. By the stable manifold theorem,

$$V_0(n) \leqslant C r_0^{-|n|}$$
 $Z_0(n) \leqslant C r_0^{-|n|}.$
(48)

As in [31, 34], we will not in general be able to solve the system (41). Instead, since $\mathbb{R}^2 = \text{span}\{V_0(0), Z_0(0)\}\$, we relax the third equation in (41) to obtain the system of equations

$$W_{i}^{\pm}(n+1) = A(n;\omega_{0})W_{i}^{\pm}(n) + [G_{i}^{\pm}(n) + (\omega - \omega_{0})B](s_{i}c_{i}V_{0}(n) + W_{i}^{\pm}(n))$$

$$W_{i}^{+}(N_{i}^{+}) - W_{i+1}^{-}(-N_{i}^{-}) = S_{i}s$$

$$W_{i}^{+}(0) - W_{i}^{-}(0) \in \mathbb{C}Z_{0}(n).$$

$$(49)$$

Using Lin's method, we will be able to find a unique solution to this system, but this solution will generically have m jumps at n = 0 in the direction of the adjoint solution $Z_0(0)$. A solution to (49) is therefore an eigenfunction if and only if the m jump conditions

$$\xi_i = \langle Z_0(0), W_i^+(0) - W_i^-(0) \rangle = 0$$
 (50)

are satisfied. Since $G_i^{\pm}(n) = \mathcal{O}(\tilde{U}_i^{\pm}(n))$, we have the same estimates for $G_i^{\pm}(n)$ as we do for \tilde{U}_i^{\pm} in (16). The terms in (49) are the same as in [34], with the addition of a term of the form $G_i^{\pm}(n)V_0(n)$. To estimate that term, we combine the estimates (16) and (48). For the interior pieces, we have

$$\begin{split} |G_i^-(n)V_0(n)| &\leqslant C r^{-N_{i-1}^-} r^{-(N_{i-1}^-+n)} r_0^n \\ &\leqslant C r^{-2N_{i-1}^-} \left(\frac{r}{r_0}\right)^{-n} \\ &\leqslant C \left(\frac{r}{r_0}\right)^{\max\{N_1,\dots,N_m\}} r^{-2N} \\ &\leqslant C r^{-2N}, \end{split}$$

where in the last step we used the fact that r_0 is fixed (it depends only on ω_0), as are the distances N_i . The constant C will be larger as r_0 decreases, which occurs as the eigenvalue λ_0 gets closer to the continuous spectrum boundary. The estimate for $G_i^+(n)V_0(n)$ is similar, and the estimates for the two exterior pieces are stronger. Thus we have the two uniform estimates

$$||G_i^{\pm}|| \leqslant Cr^{-N}$$

$$||G_i^{\pm}V_0(n)|| \leqslant Cr^{-2N}.$$
1055

The proof then follows as in [31, 34]. First, we write equation (38) as a fixed point problem using the discrete variation of constants formula together with projections on the stable and unstable subspaces of the exponential dichotomy. Let $\delta > 0$ be small, and choose N sufficiently large so that $r^{-N} < \delta$. Define the spaces

$$V_W = \ell^{\infty}([-N_{i-1}, 0]) \oplus \ell^{\infty}([0, N_i])$$

$$V_a = \bigoplus_{i=0}^{n-1} E^{\mathbf{u}} \oplus E^{\mathbf{s}}$$

$$V_b = \bigoplus_{i=0}^{n-1} \operatorname{range} P_{-}^{\mathbf{u}}(0) \oplus \operatorname{range} P_{+}^{\mathbf{s}}(0)$$

$$V_{\lambda} = B_{\delta}(\omega_0) \subset \mathbb{C}$$

$$V_s = \mathbb{R}^m.$$

Then for

$$W = (W_i^-, W_i^+) \in V_W$$
 $a = (a_i^-, a_i^+) \in V_a$
 $\lambda \in V_\lambda$ $b = (b_i^-, b_i^+) \in V_b$,

the fixed point equations for the eigenvalue problem are

$$\begin{split} W_i^-(n) &= \Phi_s^-(n, -N_{i-1}^-) a_{i-1}^- + \sum_{j=-N_{i-1}^-}^{n-1} \Phi_s^-(n, j+1) \left[G_i^-(j) \right. \\ &\quad + (\omega - \omega_0) B \right] (s_i c_i V_0(j) + W_i^-(j)) + \Phi_u^-(n, 0) b_i^- \\ &\quad - \sum_{j=n}^{-1} \Phi_u^-(n, j+1) [G_i^-(j) + (\omega - \omega_0) B] (s_i c_i V_0(j) + W_i^-(j)) \\ W_i^+(n) &= \Phi_s^+(n, 0; \theta_i) b_i^+ + \sum_{j=0}^{n-1} \Phi_s^+(n, j+1) \left[G_i^+(j) \right. \\ &\quad + (\omega - \omega_0) B \right] (s_i c_i V_0(j) + W_i^+(j)) + \Phi_u^+(n, N_i^+) a_i^+ \\ &\quad - \sum_{j=n}^{N_i^+-1} \Phi_u^+(n, j+1) [G_i^+(j) + (\omega - \omega_0) B] (s_i c_i V_0(j) + W_i^+(j)), \end{split}$$

where $a_0^- = a_m^+ = 0$, and the sums are defined to be 0 if the upper index is smaller than the lower index. We now follow the procedure in the proof of [34, theorem 2] and invert the system (49) in the following steps. First, we solve for the remainder functions $W_i^\pm(n)$ in the fixed point equations. Then, we use the second equation in (49) to solve for the initial conditions a_i^\pm . Finally, we use the third equation in (49) to solve for the b_i^\pm . The procedure is identical to that in the proof of [34, theorem 2], with both λ and λ^2 replaced by $\omega - \omega_0$, $\tilde{H}_i^\pm(n)$ replaced by $c_i V_0(n)$, and the presence of additional terms of the form $G_i^\pm(n)V_0(n)$, which will be small using the second estimate in (51) and will therefore be incorporated into the remainder term.

Thus, we obtain a unique solution to (36) which generically has n jumps in the direction of $Z_0(0)$. These jumps are given by

$$\xi_i = \langle Z_0(N_i^+), P_0^u S_i s \rangle + \langle Z_0(-N_{i-1}^-), P_0^s S_{i-1} s \rangle - (\omega - \omega_0) s_i c_i M + R(\omega - \omega_0)_i (s), \tag{52}$$

where M is the Melnikov sum

$$M = \sum_{j=-\infty}^{\infty} \langle Z_0(j+1), BV_0(j) \rangle,$$

and the remainder term has uniform bound

$$R(\omega - \omega_0)_i(s) \leqslant C \left(r^{-N} r_0^{-2N} + |\omega - \omega_0| \right) (r_0^{-N} + |\omega - \omega_0|) . \tag{53}$$

For the terms in the Melnikov sum,

$$\langle Z_0(j+1), BV_0(j) \rangle = \frac{1}{d} \langle (-v_0(j), v_0(j-1))^{\mathsf{T}}, (v_0(j), 0)^{\mathsf{T}} \rangle = -\frac{1}{d} v_0(j)^2,$$

thus it follows that

$$M = \sum_{j=-\infty}^{\infty} v_0(j)^2 = ||v_0||_{\ell^2}, \tag{54}$$

which is always positive. It follows from (45) that

$$P_0^u S_i s = s_{i+1} c_{i+1} V_0(-N_i^-) + \mathcal{O}\left(r^{-N} r_0^{-N}\right) P_0^s S_i s = -s_i c_i V_0(N_i^+) + \mathcal{O}\left(r^{-N} r_0^{-N}\right).$$

Substituting these into (52), we have

$$\xi_{i} = \langle Z_{0}(N_{i}^{+}), V_{0}(-N_{i}^{-}) \rangle s_{i+1}c_{i+1} - \langle Z_{0}(-N_{i-1}^{-}), V_{0}(N_{i-1}^{+}) \rangle s_{i-1}c_{i-1}$$

$$+ \frac{1}{d}(\omega - \omega_{0})s_{i}c_{i}M + R(\omega - \omega_{0})_{i}(d),$$

where the bound on the remainder term is unchanged. Since c_i and c_{i+1} have opposite signs, this simplifies to

$$\xi_{i} = \langle Z_{0}(N_{i}^{+}), V_{0}(-N_{i}^{-}) \rangle s_{i+1} - \langle Z_{0}(-N_{i-1}^{-}), V_{0}(N_{i-1}^{+}) \rangle s_{i-1} - \frac{1}{d}(\omega - \omega_{0}) s_{i}M + R(\omega - \omega_{0})_{i}(s).$$

Let

$$a_i = \langle Z_0(N_i^+), V_0(-N_i^-) \rangle = v_0(N_i^+)v_0(-N_i^- - 1) - v_0(N_i^+ - 1)v_0(-N_i^-).$$

Using equation (47),

$$\langle Z_0(-N_i^-), V_0(N_i^+) \rangle = v_0(N_i^+ - 1)v_0(-N_i^-) - v_0(N_i^+)v_0(-N_i^- - 1) = -a_i,$$

which we substitute above to obtain

$$\xi_i = a_i s_{i+1} + a_{i-1} s_{i-1} - \frac{1}{d} (\omega - \omega_0) s_i M + R(\omega - \omega_0)_i (s).$$
(55)

The a_i can be simplified further based on symmetries of the eigenfunction $v_0(n)$. For even, intersite eigenfunctions, $v_0(-n) = v_0(n-1)$, thus we have

$$a_i = v_0(N_i^+)v_0(N_i^-) - v_0(N_i^+ - 1)v_0(N_i^- - 1).$$
(56)

For odd, intersite eigenfunctions, $v_0(-n) = -v_0(n-1)$, and so

$$a_i = v_0(N_i^+ - 1)v_0(N_i^- - 1) - v_0(N_i^+)v_0(N_i^-).$$
(57)

This can be written as the matrix equation

$$\left(A - \frac{1}{d}(\omega - \omega_0)MI + R(\omega - \omega_0)\right)s = 0,$$
(58)

where A is defined by (25), which has a nontrivial solution if and only if

$$E(\omega - \omega_0) = \det\left(A - \frac{1}{d}(\omega - \omega_0)MI + R(\omega - \omega_0)\right)s = 0.$$
 (59)

Let $\{\mu_1, \ldots, \mu_m\}$ be the eigenvalues of A, which are real since A is symmetric. They are also distinct by [48, corollary 2.2.7], since the eigenvalue problem $(A - \mu I)v = 0$ is equivalent to the Sturm-Liouville difference equation with Dirichlet boundary conditions

$$\nabla(p_j \Delta s_j) + q_j = \mu s_j \qquad j = 1, \dots, m$$

$$s_0 = 0$$

$$s_{m+1} = 0,$$

where $p_j = a_j, q_j = a_j + a_{j-1}, \Delta$ is the forward difference operator $(\Delta f)_j = f_{j+1} - f_j$ and ∇ is the backward difference operator $(\nabla f)_j = f_j - f_{j-1}$.

Following the proof of [34, theorem 5], we can use the implicit function theorem to solve for $\omega - \omega_0$ to get the *m* solutions

$$\omega_j = \omega_0 + \frac{d\mu_j}{M} + \mathcal{O}(r_0^{-3N}) \qquad j = 1, \dots, m.$$

Since $\mu_j = \mathcal{O}(r_0^{-2N})$, $\omega_0 < 0$, and ω must be real, $\omega_j < 0$ for sufficiently small N. The corresponding eigenvalues are $\lambda_j = \pm \sqrt{\omega_j}$, which are on the imaginary axis.

ORCID iDs

Ross Parker https://orcid.org/0000-0003-2707-7334

P G Kevrekidis https://orcid.org/0000-0002-7714-3689

Alejandro Aceves https://orcid.org/0000-0002-1408-903X

References

- [1] Dodd R K, Eilbeck J C, Gibbon J D and Morris H C 1982 Solitons and Nonlinear Wave Equations 1st edn (New York: Academic)
- [2] Dauxois T and Peyrard M 2006 Physics of Solitons 1st edn (Cambridge: Cambridge University Press)

- [3] Braun O M and Kivshar Y S 2004 The Frenkel-Kontorova Model (Berlin: Springer)
- [4] Williams F 2014 The Sine-Gordon Model and Its Applications: From Pendula and Josephson Junctions to Gravity and High-Energy Physics (Nonlinear Systems and Complexity vol 10) 1st edn, ed J Cuevas-Maraver and P G Kevrekidis (Berlin: Springer)
- [5] Cuevas-Maraver J and Kevrekidis P G (ed) 2019 A dynamical perspective on the ϕ 4 model *Nonlinear Systems and Complexity* 1st edn (Berlin: Springer)
- [6] Kivshar Y S and Malomed B A 1989 Dynamics of solitons in nearly integrable systems Rev. Mod. Phys. 61 763–915
- [7] Braun O M and Kivshar Y S 1998 Nonlinear dynamics of the Frenkel–Kontorova model *Phys. Rep.* 306 1–108
- [8] Chirilus-Bruckner M, Chong C, Cuevas-Maraver J and Kevrekidis P G 2014 sine-Gordon Equation: From Discrete to Continuum *The sine-Gordon Model and its Applications* vol 10 ed J Cuevas-Maraver, P Kevrekidis and F Williams (*Nonlinear Systems and Complexity*) (Cham: Springer) pp 31–57
- [9] Karachalios N 2006 Global existence in infinite lattices of nonlinear oscillators: the discrete Klein–Gordon equation *Glasgow Math. J.* 48 200508
- [10] Scott A C 1969 A nonlinear Klein-Gordon equation Am. J. Phys. 37 52-61
- [11] Cuevas J, English L Q, Kevrekidis P G and Anderson M 2009 Discrete breathers in a forced-damped array of coupled pendula: modeling, computation, and experiment *Phys. Rev. Lett.* 102 224–101
- [12] Ustinov A V, Doderer T, Huebener R P, Pedersen N F, Mayer B and Oboznov V A 1992 Dynamics of sine-Gordon solitons in the annular Josephson junction *Phys. Rev. Lett.* 69 1815–8
- [13] Floría L M, Marín J L, Aubry S, Martínez P J, Falo F and Mazo J J 1998 Josephson-junction ladder: a benchmark for nonlinear concepts *Physica* D 113 387–96
- [14] Yomosa S 1983 Soliton excitations in deoxyribonucleic acid (DNA) double helices *Phys. Rev.* A 27 2120–5
- [15] Yakushevich L V 1998 Nonlinear Physics of DNA (Wiley Series in Nonlinear Science) (New York: Wiley)
- [16] De Leo R and Demelio S 2011 Some numerical results on motion of kinks in some model of DNA torsional dynamics Commun. Appl. Ind. Math. https://doi.org/10.1685/journal.caim.366
- [17] Heeger A J, Kivelson S, Schrieffer J R and Su W-P 1988 Solitons in conducting polymers Rev. Mod. Phys. 60 781–850
- [18] Chen D, Aubry S and Tsironis G P 1996 Breather mobility in discrete φ^4 nonlinear lattices *Phys. Rev. Lett.* 77 4776–9
- [19] Flach S and Gorbach A V 2008 Discrete breathers—advances in theory and applications Phys. Rep. 467 1–116
- [20] Ivancevic V and Ivancevic T 2013 Sine–Gordon solitons, kinks and breathers as physical models of nonlinear excitations in living cellular structures J. Geom. Symmetry Phys. 31 1–56
- [21] Segur H and Ablowitz M J 2000 Solitons and the Inverse Scattering Transform (SIAM Studies in Applied Mathematics vol 4) 1st edn (Philadelphia: Society for Industrial Mathematics)
- [22] Kevrekidis P G and Weinstein M I 2000 Dynamics of lattice kinks *Physica* D **142** 113–52
- [23] Segur H and Kruskal M D 1987 Nonexistence of small-amplitude breather solutions in phi⁴ theory Phys. Rev. Lett. 58 747–50
- [24] Peyrard M and Kruskal M D 1984 Kink dynamics in the highly discrete sine-Gordon system *Physica* D 14 88–102
- [25] Kevrekidis P G 2009 The Discrete Nonlinear Schrödinger Equation (Berlin: Springer)
- [26] Aigner A A, Champneys A R and Rothos V M 2003 A new barrier to the existence of moving kinks in Frenkel–Kontorova lattices *Physica* D 186 148
- [27] Iooss G and Pelinovsky D E 2006 Normal form for travelling kinks in discrete Klein–Gordon lattices Physica D 216 327
- [28] Cisneros L A and Minzoni A A 2008 Asymptotics for kink propagation in the discrete sine-Gordon equation *Physica* D 237 50
- [29] Pelinovsky D and Sakovich A 2012 Multi-site breathers in Klein-Gordon lattices: stability, resonances and bifurcations Nonlinearity 25 3423-51
- [30] Cuevas J, Koukouloyannis V, Kevrekidis P G and Archilla J F R 2011 Multibreather and vortex breather stability in Klein–Gordon lattices: equivalence between two different approaches *Int. J. Bifurcation Chaos* 21 2161–77
- [31] Sandstede B 1998 Stability of multiple-pulse solutions Trans. Am. Math. Soc. 350 429-72

- [32] Lin X-B 1990 Using Melnikov's method to solve Silnikov's problems *Proc. R. Soc. Edinburgh* A 116 295–325
- [33] Lin X-B 2008 Lin's method Scholarpedia 3 6972
- [34] Parker R, Kevrekidis P G and Sandstede B 2020 Existence and spectral stability of multi-pulses in discrete Hamiltonian lattice systems *Physica* D 408 132414
- [35] Parker R and Aceves A 2021 Multi-pulse solitary waves in a fourth-order nonlinear Schrödinger equation *Physica* D 422 132890
- [36] Knobloch J 2000 Lin's method for discrete dynamical systems J. Diff. Equ. Appl. 6 577-623
- [37] Kapitula T, Kevrekidis P G and Malomed B A 2001 Stability of multiple pulses in discrete systems Phys. Rev. E 63 036604
- [38] Balmforth N J, Craster R V and Kevrekidis P G 2000 Being stable and discrete Physica D 135 212–32
- [39] Kapitula T and Kevrekidis P 2001 Stability of waves in discrete systems Nonlinearity 14 533-66
- [40] Kivshar Y S, Pelinovsky D E, Cretegny T and Peyrard M 1998 Internal modes of solitary waves Phys. Rev. Lett. 80 5032–5
- [41] Manton N S 1979 An effective Lagrangian for solitons Nucl. Phys. B 150 397-412
- [42] Hairer E, Lubich C and Wanner G 2006 Geometric Numerical Integration (Springer Series in Computational Mathematics vol 31) (Berlin: Springer)
- [43] Duncan D B 1997 Sympletic finite difference approximations of the nonlinear Klein–Gordon equation SIAM J. Numer. Anal. 34 1742–60
- [44] Hairer E and Hairer M 2003 GniCodes—Matlab programs for geometric numerical integration Frontiers in Numerical Analysis (Berlin: Springer) ed J F Blowey, A W Craig and T Shardlow pp 199–240
- [45] Kevrekidis P G 2003 On a class of discretizations of Hamiltonian nonlinear partial differential equations *Physica* D **183** 68–86
- [46] Barashenkov I V and van Heerden T C 2008 Exceptional discretizations of the sine-Gordon equation Phys. Rev. E 77 036601
- [47] Takeno S and Homma S 1986 A sine-lattice (sine-form discrete sine-Gordon) equation one-and two-kink solutions and physical models J. Phys. Soc. Japan 55 198601
- [48] Jirari A 1995 Second-Order Sturm-Liouville Difference Equations and Orthogonal Polynomials (Providence, RI: American Mathematical Society)